Smart Mater. Struct. **20** (2011) 055020 (10pp) doi:10.1088/0964-1726/20/5/055020

The pyroelectric energy harvesting capabilities of PMN–PT near the morphotropic phase boundary

Razmig Kandilian, Ashcon Navid and Laurent Pilon[1]

Mechanical and Aerospace Engineering Department, Henry Samueli School of Engineering and Applied Science, University of California, Los Angeles, Los Angeles, CA 90095, USA

E-mail: pilon@seas.ucla.edu

Received 30 December 2010, in final form 10 March 2011
Published 19 April 2011
Online at stacks.iop.org/SMS/20/055020

Abstract

This paper reports on direct thermal to electrical energy conversion by performing the Olsen cycle on pyroelectric materials. The energy harvesting capability of commercially available [001] oriented $68PbMg_{1/3}Nb_{2/3}O_3$–$32PbTiO_3$ (PMN–32PT) single crystal capacitors was measured experimentally. An energy density of 100 mJ cm^{-3}/cycle, corresponding to 4.92 mW cm^{-3}, was obtained by successively dipping the material in oil baths at temperatures 80 and 170 °C and cycling the electric field between 2 and 9 kV cm^{-1}. Similarly, an energy density of 55 mJ cm^{-3}/cycle was obtained between 80 and 140 °C. An estimated 40% of this energy resulted from the strain polarization due to the rhombohedral to tetragonal phase transition. The strain from this transition disappeared when the maximum operating temperature exceeded the Curie temperature of about 150 °C. The optimal low electric field used in the Olsen cycle maximizing the energy harvested was found to be around 2 kV cm^{-1}. In addition, the material suffered from (i) dielectric breakdown for electric fields larger than 9 kV cm^{-1} and (ii) cracking from thermal stress for operating temperature differences in excess of 90 °C. A physical model predicting the total amount of energy harvested was also derived, accounting for thermal expansion as well as temperature dependent dielectric constant and spontaneous polarization. The model predictions fell within 20% of the experimental results in the temperature range between 80 and 170 °C and electric fields ranging from 2 to 9 kV cm^{-1}.

1. Introduction

Recent societal trends towards environmentally friendly technologies and renewable energy sources have revived interest in increasing efficiency of existing processes and harvesting the waste heat they produce. As a direct consequence of the second law of thermodynamics, large amounts of low grade (low temperature) waste heat is produced in power generation, heating, refrigeration, and other industrial processes. It is estimated that over 50% of the energy consumed in the United States in 2009 was lost in the form of low grade waste heat, 85% of which comes from electrical power generation and transportation systems [1]. Typical transportation systems have energy efficiencies of 30–40%. In other words, 60–70% of the energy contained in the fuel is wasted by releasing waste heat [2]. In fact, the temperature of the exhaust gas from internal combustion engines ranges between 200 and 500 °C while the engine oil is usually maintained at 125–150 °C [3]. Studies in the past several decades have focused on converting waste heat directly to electricity by using thermoelectric devices which operate under a steady-state temperature gradient [4]. In contrast, pyroelectric devices require temporal temperature oscillations in order to directly convert thermal energy into electrical energy. Using pyroelectric materials, it is possible to produce electricity from waste heat in the temperature range from 25 to 200 °C [5–19]. Several devices have been designed, assembled and operated to produce temperature oscillations for pyroelectric waste heat harvesting [6, 8–10, 20–22]. In order to increase their efficiency and the electrical energy harvested, it is necessary to identify the best material for the temperature range considered.

[1] Author to whom any correspondence should be addressed.

The present study reports experimental measurements of the energy harvested by applying the Olsen cycle on commercially available [001] oriented $68PbMg_{1/3}Nb_{2/3}O_3$–$32PbTiO_3$ (PMN–32PT) single crystal capacitors. Simultaneously a physical model was developed and compared with experimental data in order to identify parameters that are important in the heat to electricity conversion process.

2. Background

2.1. Pyroelectricity and ferroelectricity

Pyroelectric materials possess a so-called spontaneous polarization, denoted by P_s in the absence of an electric field. In addition, ferroelectric materials are pyroelectric materials whose spontaneous polarization can be reversed by applying an electric field. This spontaneous polarization strongly depends on temperature. In fact, when heated above the Curie temperature, denoted by T_{Curie}, ferroelectric materials undergo a phase transition into paraelectric state and no longer possess a spontaneous polarization. When cooled below T_{Curie}, the material undergoes a structural transformation into a ferroelectric state and regains its spontaneous polarization [23]. In the absence of a phase transition, the electric displacement D of the material at temperature T is defined as a function of the applied electric field E and its spontaneous polarization P_s [24]

$$D(E,T) = \varepsilon(T)E + P_s(T) \quad (1)$$

where ε is the dielectric permittivity. Figure 1 shows typical D–E curves for relaxor ferroelectric materials at two different temperatures. The D–E curve for temperature T_{hot} is characteristic of a paraelectric material with P_s approximately 0 C m^{-2}. The curve at temperature T_{cold} shows the material having a so-called remnant polarization P_r in the absence of an electric field. However, it regains its spontaneous polarization P_s when an electric field of a certain magnitude is applied as illustrated in figure 1 [25]. This remnant polarization is significantly lower than the spontaneous polarization.

Relaxor ferroelectric materials such as PMN–PT have a so-called diffuse ferro-to-paraelectric phase transition, i.e., they undergo phase transitions over a wide temperature range. The crystal structure and the Curie temperature of PMN–PT depend on the ratio of relaxor PMN to ferroelectric PT [25]. For PMN–32PT with [001] poling, the Curie temperature is 150 °C and the crystal structure at room temperature is rhombohedral which transitions to tetragonal at around 80 °C and finally to cubic at 150 °C [26].

Both pyroelectric and ferroelectric materials are also piezoelectric. Piezoelectrics are materials whose internal polarization can be changed by straining it [23]. PMN–PT with a $PbTiO_3$ composition ranging from 28 to 32% is near the so-called morphotropic phase boundary (MPB) which is characterized by very large electro-mechanical properties [25].

2.2. Pyroelectric energy conversion

2.2.1. Olsen cycle. The Olsen cycle, applied to pyroelectric materials, consists of two isothermal and two isoelectric field processes [8]. It is analogous to the Ericsson cycle which consists of two isothermal and two isobaric processes on a working fluid [27]. Figure 1 presents a typical Olsen cycle in the electric displacement versus electric field diagram (D–E diagram). The area enclosed by the Olsen cycle is the electrical energy produced per unit volume of material per cycle. Process 1–2 consists of increasing the electric field from E_L to E_H isothermally at temperature T_{cold}. Process 2–3 corresponds to heating of the material from temperature T_{cold} to T_{hot} under constant electric field E_H. Process 3–4 consists of reducing the electric field from E_H to E_L under isothermal conditions at T_{hot}. Finally, the cycle is closed by cooling the material to T_{cold} under constant electric field E_L. In brief, the principle of the Olsen cycle is to charge a capacitor through cooling under low electric field and to discharge it through heating under higher field.

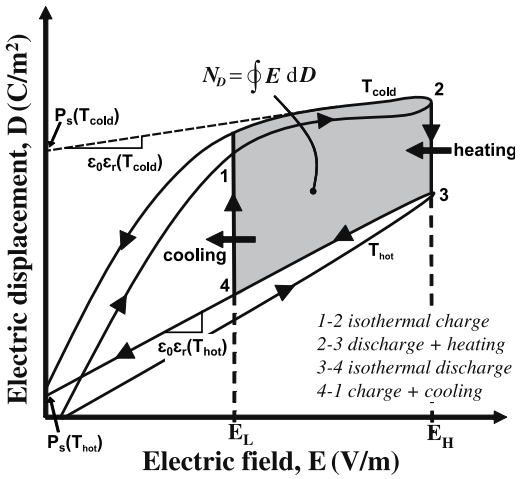

Figure 1. Electric displacement versus electric field for a typical pyroelectric material at temperatures T_{hot} and T_{cold} along with the Olsen cycle. The electrical energy generated per cycle is represented by the area enclosed by 1–2–3–4.

In the early 1980s, Olsen and co-workers adapted the Ericsson cycle to pyroelectric converters using PZST [9] and P(VDF-TrFE) [5, 28] thin films. Olsen *et al* [7] reviewed the different cycles they tested and noted that the Carnot cycle was the most efficient but the least practical. They showed experimentally that what is now called the Olsen cycle [13] harvested the largest energy density compared to resistive, two-diode, Stirling and Carnot cycles [7]. Furthermore, Olsen *et al* [6] established that, by using the Olsen cycle with regeneration, the efficiency of the converter could reach the Carnot efficiency. Pilon and co-workers [14, 29] numerically simulated a prototypical pyroelectric converter based on the design and operation proposed by Olsen *et al* [6] and showed that it was possible to achieve 55% of Carnot efficiency [14].

2.2.2. Experimental studies. Successively dipping the pyroelectric film into hot and cold baths under the specified electric fields provides a simple and somewhat idealized way of performing the Olsen cycle. It can be used as a method to assess the performance of materials before integrating them into actual devices. Olsen *et al* [5] performed the Olsen

cycle on 70–100 μm thick 60/40 P(VDF-TrFE) films by successively dipping the film into cold and hot silicone oil baths maintained at 25 °C and 100–120 °C, respectively [5]. The low electric field E_L was set at 200 kV cm^{-1} while the high electric field E_H varied between 200 and 600 kV cm^{-1}. The maximum amount of energy harvested was reported to be 900 mJ cm^{-3} of pyroelectric material per cycle corresponding to 112.5 mW cm^{-3} of material [5].

Ikura [13] also performed the Olsen cycle on 25 μm thick 60/40 P(VDF-TrFE) films subjected to a periodic flow of hot and cold water at 58 and 77 °C, respectively. The author reported an energy density between 15 and 52 mJ cm^{-3}/cycle. Kouchachvili and Ikura [11, 12] reported an energy density of 279 mJ cm^{-3}/cycle [11] using 60/40 P(VDF-TrFE) purified by a proprietary process [12]. However, the working fluid and operating temperatures and frequency were not specified.

More recently, Navid *et al* [15] experimentally found the energy densities of commercial, purified and porous 60/40 P(VDF-TrFE) to be 521, 426, and 188 mJ cm^{-3}/cycle, respectively. Nguyen *et al* [21] designed and assembled a prototypical device using commercial 60/40 P(VDF-TrFE) and 50 cSt silicone oil as the working fluid. The authors achieved 130 mJ cm^{-3}/cycle by operating the device between $T_{cold} = 70$ °C and $T_{hot} = 110$ °C and between $E_L = 200$ kV cm^{-1} and $E_H = 400$ kV cm^{-1} at 0.1 Hz frequency [21].

Ceramic and single crystal ferroelectric materials have also been used to directly convert heat into electricity. Unlike polymers, ceramics present the advantage of being able to withstand high temperatures without melting. For example, Olsen [9] used PZST ceramic samples in a pyroelectric generator and obtained 100 mJ cm^{-3}/cycle working between 146 and 159 °C and electric field spanning from 0 to 29 kV cm^{-1}. Moreover, ceramics and single crystals such as $(1-x)$PMN–xPT and $(1-x)PbZn_{1/3}Nb_{2/3}O_3$–$xPbTiO_3$ (PZN–PT) have received significant attention for their potential in waste heat energy harvesting [16–19, 30]. Sebald *et al* [16] evaluated the energy harvesting capabilities of 0.9PMN–0.1PT bulk ceramics and reported a maximum energy density of 186 mJ cm^{-3}/cycle by performing dipping experiments between 35 and 85 °C with electric field cycling between 0 and 30 kV cm^{-1}. Similarly, Zhu *et al* [19] achieved 216.5 mJ cm^{-3}/cycle by dipping single crystal PZN–4.5PT between 100 and 160 °C with a maximum electric field of 20 kV cm^{-1}. Khodayari *et al* [18] also used PZN–4.5PT single crystals to assess the amount of energy harvested due to phase transition through rhombohedral, orthorhombic, and tetragonal phases during the Ericsson cycle. The authors obtained 101.8 mJ cm^{-3}/cycle operating between temperatures 100 and 130 °C and electric fields between 0 and 20 kV cm^{-1} [18].

2.2.3. Physical modeling of the Olsen cycle. The only previous effort to model the energy harvested during the Olsen (or Ericsson) cycle was reported by Sebald *et al* [16] for PMN–PT. The authors assumed the pyroelectric coefficient p and the dielectric permittivity ε to be constant in the operating temperature range from 35 to 105 °C. Then, the energy density of the cycle was expressed as [16],

$$N_D = (T_{hot} - T_{cold}) \int_{E_L}^{E_H} p \, dE = p(T_{hot} - T_{cold})(E_H - E_L). \quad (2)$$

Unfortunately, the authors did not provide the values of the constant properties used and the model predictions were not compared with experimental measurements [16].

By contrast, the present study aims to (i) experimentally evaluate the capabilities of PMN–32PT single crystals at harvesting waste heat using the Olsen cycle, (ii) develop a physical model for the Olsen cycle accounting for temperature dependent physical properties, and (iii) directly compare the model predictions with experimental results.

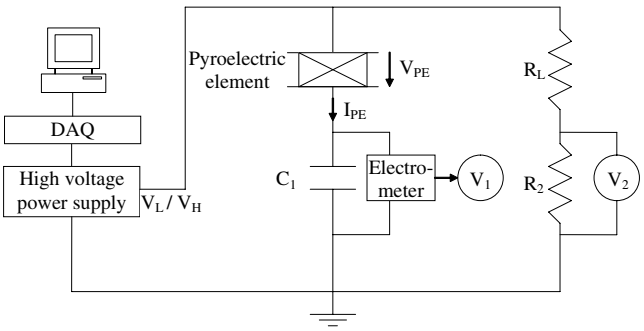

Figure 2. Electrical circuit used in the present study to perform the Olsen cycle and to measure the D–E loops at different temperatures. (This figure is in colour only in the electronic version)

3. Experiments

3.1. Materials

Six single crystal 68PMN–32PT samples poled in the [001] direction were acquired from Sinoceramics, State College, PA [31]. The sample surface area A and thickness b were 1 cm^2 and 140 μm, respectively. The samples were coated with Cr/Au electrodes on both sides. Electrical wires were attached to the electrodes using conductive silver epoxy.

3.2. Experimental setup and procedure

The experimental apparatus required to perform the Olsen cycle consisted of a thermal and an electrical subsystems. Figure 2 shows the electrical subsystem consisting of a Sawyer–Tower circuit [24] used to apply the required electric field and to collect the charges. A resistive voltage divider was placed in parallel to the Sawyer–Tower bridge to monitor the electric field applied to the material. The voltage V_1 across the capacitor C_1 was measured using a Burr-Brown DIFET electrometer (OPA128) to minimize discharge of the capacitor connected to an IOtech 3000 series data acquisition system (DAQ). The resistor R_L acted as a voltage divider to scale the voltage across the resistor R_2 in order to match the maximum voltage input of 10 V of the DAQ. The electric field was applied by a computer generated function through the DAQ connected to a TREK 610E high voltage power supply. The magnitudes

of the displacement and electric field across the PMN–32PT samples were calculated as follows

$$D = \frac{Q}{A} = \frac{C_1 V_1}{A} \qquad \text{and}$$
$$E = \frac{V_{\mathrm{PE}}}{b} = \frac{V_2(1 + R_{\mathrm{L}}/R_2) - V_1}{b}. \tag{3}$$

The thermal subsystem used to impose the temperatures T_{cold} and T_{hot} consisted of two glass beakers filled with Dow Corning 200 cSt dielectric silicone oil. The baths were maintained at constant temperatures by temperature controlled hot plates. J-type thermocouples were immersed in the fluid to monitor and record the baths' temperatures. To create the time dependent temperature oscillations, the samples were alternately dipped in the hot and cold baths. Once the sample was immersed in the oil bath, sufficient time (∼10 s) was allowed for the sample's electric displacement to reach steady-state (i.e., $\partial D/\partial t = 0$) before transferring the sample from one bath to the other.

The Olsen cycle was performed for various values of electric fields E_{L} and E_{H}, and hot temperature T_{hot}. The minimum and maximum electric fields were respectively varied from 0 to 3 kV cm^{-1} and from 4 to 9 kV cm^{-1} to explore their effects on the amount of energy harvested. The Curie temperature of the material, reported by the supplier, was 150 °C in absence of electric field. The cold bath temperature T_{cold} was maintained at 80 °C and that of the hot bath T_{hot} varied from 130 to 170 °C. The temperature T_{hot} was tested both above and below the Curie temperature in order to explore the effects of the different phase transitions on the amount of energy harvested.

Displacement versus electric field hysteresis curves were also measured at T_{cold} and T_{hot} in order to examine the relationship between temperature dependent D–E loops and the Olsen cycle. The D–E loops were measured using the same electrical circuit used as that shown in figure 2. The sample was first immersed in silicone oil at room temperature and then heated to the desired temperature. The D–E loop measurements were performed once the temperature was stabilized at $T_{\mathrm{cold}} = 80$ °C and T_{hot} between 130 and 170 °C with 10 °C increments. The maximum electric field used for the D–E loop measurements was 6 kV cm^{-1} to ensure that the material did not break during the measurements. A continuous triangular wave at frequency 0.1 Hz was applied to the film by the high voltage power supply.

4. Analysis

This section aims to develop a physical model that predicts the amount of energy harvested during the Olsen cycle. The model will be used to identify the major physical phenomena taking place in the cycle and the material properties important to the energy conversion process. The model will then be used to make quantitative predictions for the energy harvested during the Olsen cycle based on the intrinsic properties of the material.

4.1. Modeling the energy density of the Olsen cycle

The energy density harvested per cycle N_D is represented by the area enclosed by the Olsen cycle plotted in the D–E diagram. It is calculated by integrating the elementary electrical work $E\,\mathrm{d}D$ over the cycle, i.e. [8],

$$N_D = \oint E\,\mathrm{d}D. \tag{4}$$

Similarly, the power density P_D, expressed in mW cm^{-3}, is the amount of energy generated by the pyroelectric material per unit volume per unit time and is given by $P_D = N_D/\tau$ where τ is the cycle period.

For an unclamped ferroelectric material with polar axis in the direction perpendicular to the planar electrodes, the elementary change in the electric displacement can be written as [24]

$$\mathrm{d}D = \varepsilon\,\mathrm{d}E + p\,\mathrm{d}T. \tag{5}$$

The dielectric permittivity can be expressed as $\varepsilon = \varepsilon_{\mathrm{r}}\varepsilon_0$ where ε_{r} is the relative permittivity of the material and ε_0 is the vacuum permittivity equal to 8.854×10^{-12} F m^{-1}. The term p is the pyroelectric coefficient in μC cm^{-2} defined as $p = (\partial D/\partial T)$. For an unclamped crystal, it consists of two terms, namely (i) the primary pyroelectric coefficient accounting for changes in crystal dipole moment and (ii) the secondary pyroelectric coefficient due to dimensional changes in the crystal both caused by changes in temperature [24]. The unclamped pyroelectric coefficient under constant stress X and electric field E can be written as [23, 24]

$$p = \left(\frac{\partial D}{\partial T}\right)_{X,E} = p^{x,E} - \frac{d_{33}\alpha_3}{s_{33}} \tag{6}$$

where $p^{x,E}$ is the primary pyroelectric coefficient, i.e., under constant strain x and electric field E. Likewise, the second term on the right-hand side of equation (6) is the secondary pyroelectric coefficient due to thermal expansion [24]. It corresponds to the piezoelectric contribution to the pyroelectric effect. Here $\alpha_3 = x_3/\Delta T$ is the thermal expansion coefficient, expressed in K^{-1}, equal to the strain x_3 resulting from temperature change ΔT. Similarly, d_{33} is the piezoelectric coefficient in C/N and s_{33} is the elastic compliance and has units of m^2 N^{-1} [24]. The secondary pyroelectric coefficient vanishes when the material is clamped and not allowed to expand, i.e. $\alpha_3 = 0.0$ K^{-1} [24]. For isoelectric field processes 2–3 and 4–1, the first term is equal to zero while for isothermal processes 1–2 and 3–4 the second term on the right-hand side of equation (5) vanishes. Thus, equation (4) can be integrated piecewise over the four processes to obtain the energy density per cycle

$$N_D = \int_{E_{\mathrm{L}}}^{E_{\mathrm{H}}} \varepsilon_0\varepsilon_{\mathrm{r}}(E, T_{\mathrm{cold}})E\,\mathrm{d}E + E_{\mathrm{H}}\int_{T_{\mathrm{cold}}}^{T_{\mathrm{hot}}} p(E_{\mathrm{H}}, T)\,\mathrm{d}T + \int_{E_{\mathrm{H}}}^{E_{\mathrm{L}}} \varepsilon_0\varepsilon_{\mathrm{r}}(E, T_{\mathrm{hot}})E\,\mathrm{d}E + E_{\mathrm{L}}\int_{T_{\mathrm{hot}}}^{T_{\mathrm{cold}}} p(E_{\mathrm{L}}, T)\,\mathrm{d}T. \tag{7}$$

The difficulty in modeling the energy generated by the Olsen cycle lies in the fact that the properties are strongly dependent on electric field and temperature. Furthermore,

Table 1. PMN–32PT [001] properties reported in literature used in equations (2) and (10) to predict the energy density harvested during the Olsen cycle.

Properties	Units								Reference
Temperature	(°C)	23	80	130	140	150	160	170	
p	(μC m^{-2} K^{-1})	390[a]	800	4000[a]	5500[a]	7300[a]	4730[a]	910[a]	[34]
P_s	(μC cm^{-2})	—	19.6	16.7	12.6	4.98	2.79	2.43	[26]
ε_r	—	—	6000	5400	5750	14 500	16 000	15 000	[26]
d_{33}	(pC N^{-1})	1857	—	—	—	—	—	—	[33]
s_{33}	(pm^2 N^{-1})	80	—	—	—	—	—	—	[33]
x_3 (from 80 °C to T)	(%)	—	0.0	0.11	0.11	0.0	0.0	0.0	[32]

[a] Values are presented for the sake of completeness and were not used for model predictions.

the material suffers from electrical and thermal hysteresis making it difficult to match measured properties with operating conditions. Therefore, further assumptions need to be made to simplify the equations as discussed in section 4.2.

4.2. Temperature dependent properties

Near the phase transition, the properties of pyroelectric materials change appreciably with temperature [23]. Thus, temperature effects on the material properties cannot be ignored.

The change in the electric displacement defined by equation (1) with respect to temperature is the primary pyroelectric coefficient given by [23]

$$p^{x,E} = \left(\frac{\partial D}{\partial T}\right)_{x,E} = \varepsilon_0 \frac{\partial \varepsilon_r}{\partial T} E + \frac{\partial P_s}{\partial T}. \tag{8}$$

The first and second term of the right-hand side of equation (8) are the dielectric and dipole contribution to the primary pyroelectric coefficient, respectively. By adding the secondary pyroelectric term the unclamped pyroelectric coefficient can be expressed as

$$p = p^{x,E} + \frac{d_{33}\alpha_3}{s_{33}} = \varepsilon_0 \frac{\partial \varepsilon_r}{\partial T} E + \frac{\partial P_s}{\partial T} - \frac{d_{33}\alpha_3}{s_{33}}. \tag{9}$$

Combining equations (7) and (9) and carrying out the integration gives the energy density generated from an Olsen cycle as

$$N_D = (E_H - E_L)\left\{\frac{\varepsilon_0}{2}[\varepsilon_r(T_{cold}) - \varepsilon_r(T_{hot})](E_H + E_L) + \left[P_s(T_{cold}) - P_s(T_{hot}) + \frac{d_{33}x_3}{s_{33}}\right]\right\} \tag{10}$$

where $x_3 = \alpha_3(T_{hot} - T_{cold})$ as previously mentioned. Note that, if the pyroelectric coefficient p is assumed to be independent of temperature and electric field, equation (10) reduces to equation (2).

4.3. Constitutive relationships

Table 1 summarizes the properties used to compute the energy density predicted by the physical models given by equations (2) and (10). Unfortunately, the supplier was not able to provide all the material properties used in these models. Therefore, properties reported in literature [26, 32–34] for PMN–32PT with [001] poling were used in the model predictions. The relative permittivity $\varepsilon_r(T)$ and spontaneous polarization $P_s(T)$ of [001] poled PMN–32PT as a function of temperature were found in the literature [26]. The authors measured P_s by taking the intercept of the linear portion of the hysteresis curve at zero electric field. Note that their data showed that the remnant and spontaneous polarizations were approximately the same for the temperature and electric field considered in the present study. The relative permittivity was measured under DC electric field of 5 kV cm^{-1} [26]. This falls in the range of operating conditions of the present study. Thermal expansion and strain data was also found in literature for [001] poled PMN–32PT [32]. Finally, the piezoelectric coefficient d_{33} and elastic compliance s_{33} for PMN–32PT [001] at room temperature were reported by Yasuda *et al* [33].

4.4. Discussion

According to equation (10) it is possible to increase the energy density by increasing the electric field span ($E_H - E_L$). In the present study, the PMN–32PT samples used were able to withstand E_H up to 9 kV cm^{-1}. Beyond 9 kV cm^{-1}, the samples cracked or their electrical conductivity increased possibly due to micro-crack development in the structure. To address this limitations, thin films with thickness on the order of a few hundred nanometers could be used as they have been shown to withstand electric fields 10–100 times larger than their bulk counterparts [35].

The second way to increase the energy harvested is to increase the change in displacement. For a given material, it can be increased by increasing the difference between T_{cold} and T_{hot}. However, excessive temperature difference results in thermal stresses and potential cracking of the sample. Furthermore, increasing the temperature beyond the Curie temperature does not result in appreciable energy gain as demonstrated in the subsequent sections. Alternatively, ferroelectric materials with larger pyroelectric coefficient and spontaneous polarization need to be synthesized in order to increase this parameter. The term $[\varepsilon_r(T_{cold}) - \varepsilon_r(T_{hot})]$ accounts for the change in dielectric permittivity with respect to temperature. The dielectric permittivity typically increases as a function of temperature until it reaches the Curie temperature beyond which it starts decreasing [24, 26]. However, the term $[\varepsilon_r(T_{cold}) - \varepsilon_r(T_{hot})]$ becomes negligible above a certain electric field once the relative permittivity is saturated as the dipoles align themselves in the direction of the electric field [24, 26]. In this region, the relative permittivity at all temperatures is approximately constant and this term can be neglected [26].

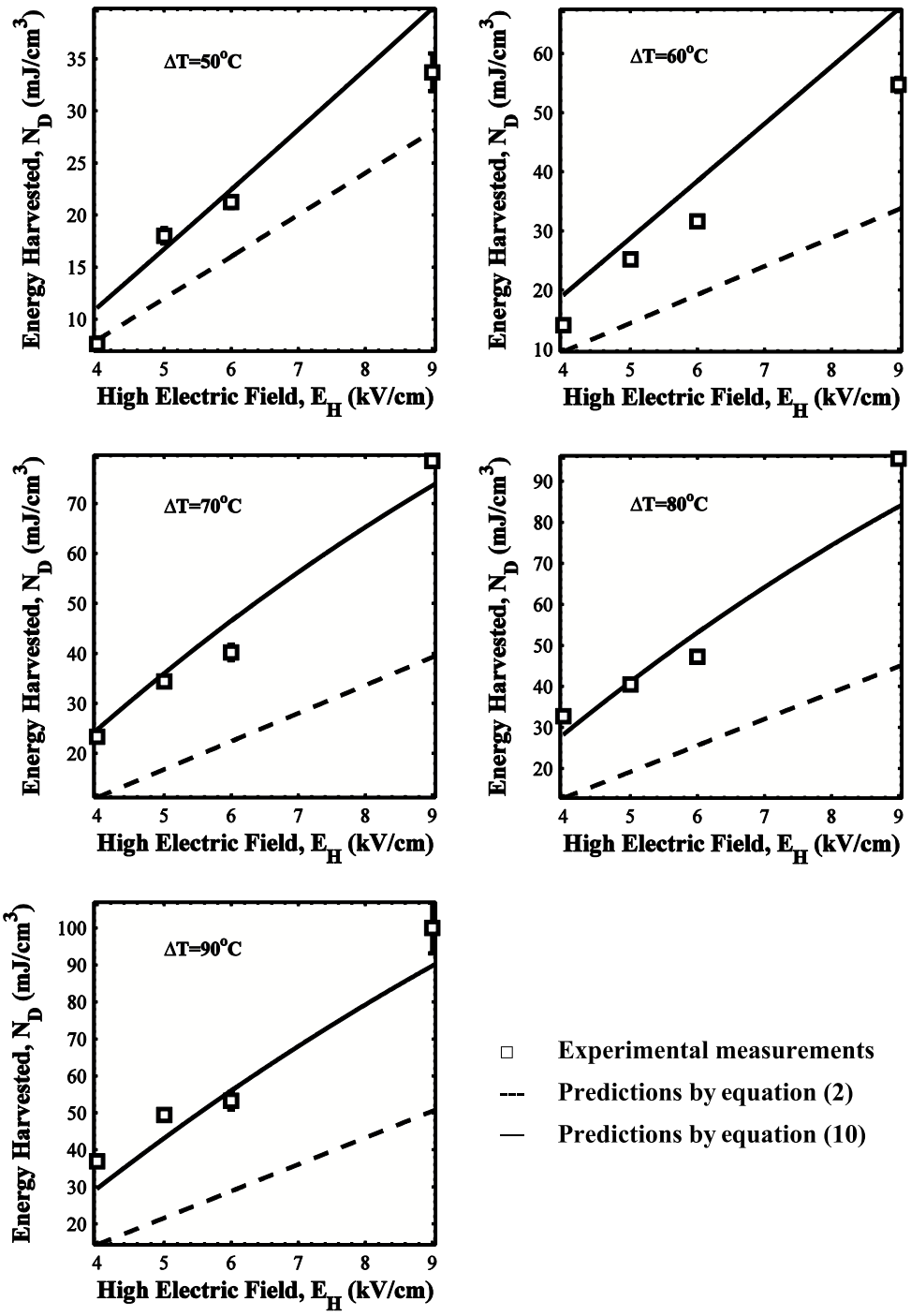

Figure 3. Experimentally measured energy density harvested with PMN–32PT single crystals versus high electric field E_H for different values of $\Delta T = T_{hot} - T_{cold}$. The temperature T_{cold} was maintained at 80 °C and the low electric field E_L was set at 2.0 kV cm^{-1}. The dashed and solid lines correspond to predictions by equations (2) and (10), respectively.

The samples used in this study were not able to withstand electric fields large enough to observe this behavior.

5. Results and discussion

5.1. Experimental results

Figure 3 shows the energy density harvested per unit volume of PMN–32PT as a function of electric field E_H for different temperatures T_{hot}. The electric field E_L was fixed at 2.0 kV cm^{-1} and the cold temperature T_{cold} was maintained at 80 °C for all experiments. All experimental data reported in figure 3 were obtained with the same sample and were averaged over five cycles. The error bars correspond to a 95% confidence interval. The largest amount of energy harvested from this sample was 100 mJ cm^{-3}/cycle, corresponding to 4.92 mW cm^{-3}, obtained between temperatures $T_{cold} = 80$ °C and $T_{hot} = 170$ °C and electric fields $E_L = 2$ kV cm^{-1} and $E_H = 9$ kV cm^{-1}.

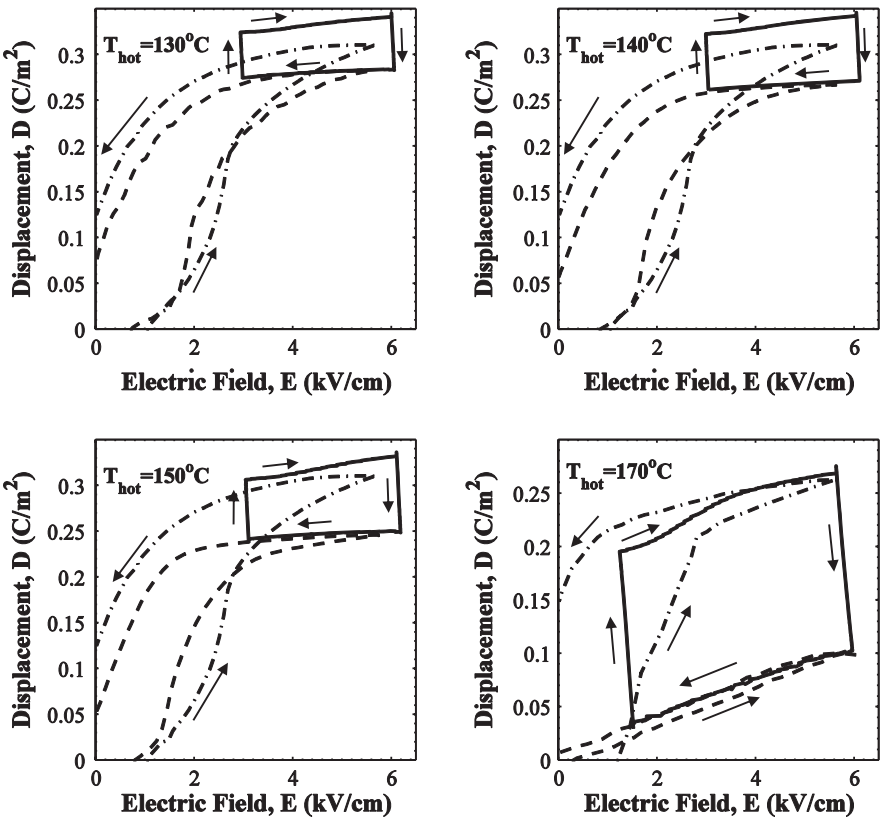

Figure 4. *D–E* curves and Olsen cycle performed at temperatures T_{cold} and T_{hot}. Dash-dotted lines (— · —) correspond to *D–E* curves at $T_{cold} = 80\,^{\circ}C$. Dashed lines (- - - -) correspond to *D–E* loops for T_{hot} equal to 130, 140, 150 and 170 °C. Solid lines correspond to the Olsen cycles performed between 80 °C and T_{hot}. The Olsen cycle is displaced to coincide with *D–E* curve at T_{hot}.

Note that differences in energy density harvested from one sample to another were large and could reach up to 50%. Both the spontaneous polarization and the Curie temperature also varied significantly which resulted in different performances. For example, the spontaneous polarization was 23 μC cm^{-2} for one sample at room temperature and 30 μC cm^{-2} for another. Similarly, one sample had transitioned to cubic phase (paraelectric) by 160 °C while another was still ferroelectric at 170 °C.

5.1.1. Effects of temperature and phase transitions. As previously discussed, PMN–32PT with [001] orientation undergoes two solid phase transitions [26, 32] namely (i) from rhombohedral to tetragonal structures at around 80 °C and (ii) from tetragonal to cubic structures at around 150 °C. Additionally, thermal expansion is only significant when the material undergoes a phase transition [32]. For example, the strain x_3 resulting from thermal expansion between 80 and 120 °C was found to be 0.11% but was negligible when no phase transition occurred [32]. Between $T_{cold} = 80\,^{\circ}C$ and $T_{hot} \geqslant 130\,^{\circ}C$, the PMN–32PT samples underwent rhombohedral to tetragonal phase transition. However, only those with $T_{hot} \geqslant T_{Curie}$ transitioned from tetragonal to cubic structures. This section compares the Olsen cycle and *D–E* loops in order to evaluate the relative importance of primary and secondary pyroelectric coefficients along with the phase transition effects on the energy density harvested.

In order to facilitate the comparison, equilibrium *D–E* curves were obtained at different temperatures and compared with the Olsen cycle. The equilibrium *D–E* curve plots equation (1) at temperatures T_{cold} and T_{hot}. For a given electric field say E_L or E_H, the difference in the electric displacement ΔD between the *D–E* loop at T_{cold} and that at T_{hot} corresponds to the primary pyroelectric coefficient as per equation (8). On the other hand, the isoelectric field processes in the Olsen cycle include both primary and secondary pyroelectric effects which are accounted for by equation (9). Comparing ΔD between the *D–E* loops and the Olsen cycle enable the discrimination between the primary and the secondary pyroelectric effects. Note that the cycle and *D–E* loop measurements were performed on the same sample in order to avoid uncertainty resulting from sample variation.

Figure 4 shows the displacement versus electric field for bipolar hysteresis curves at temperatures $T_{cold} = 80\,^{\circ}C$ and T_{hot} equals to 130, 140, 150, and 170 °C for electric fields $E_L = 3$ kV cm^{-1} and $E_H = 6$ kV cm^{-1}. It also plots the Olsen cycle operating between these two temperatures. Due to the measurement method of the electric displacement when performing the Olsen cycle, it was only possible to measure changes in electric displacement ΔD rather than the absolute displacement D. In order to compare the Olsen cycle with the equilibrium *D–E* curves, the cycle was translated vertically to coincide with the *D–E* loop measured at T_{hot}. Figure 4 establishes that for $T_{hot} = 130$ and 140 °C, the change in

electric displacement observed during the Olsen cycle was larger than the change in displacement between the two *D*–*E* curves at temperatures T_{hot} and T_{cold}. This can be attributed to the secondary pyroelectric effect which contributed about 40% of the total change in displacement. However, when T_{hot} was set larger than $T_{Curie} = 150\,^{\circ}C$, the strain polarization due to thermal expansion vanished. We speculate that this can be attributed to thermal hysteresis. Indeed, according to Li *et al* [32], a [001] poled PMN–32PT has two different strains depending on the operating conditions. When the sample is heated from 80 °C to temperature below T_{Curie}, the strain due to tetragonal to rhombohedral phase transition is 0.11% [32]. In contrast, when the PMN–32PT is cooled from above T_{Curie} down to 80 °C, the strain due to tetragonal to rhombohedral transition is 0.02% [32]. In addition, the piezoelectric coefficient for unpoled material is significantly less than that for a poled material [25] and is negligible near the Curie temperature. Moreover, experimentally, there was no difference in the relative permittivity of the material measured in the linear region with respect to electrical or thermal hysteresis. Therefore, change in the relative permittivity value was ruled out as the cause for the change in the displacement observed beyond the change in the spontaneous polarization.

Therefore, beyond the Curie temperature the strain polarization is significantly smaller and can be neglected. This implies that (i) having PMN–32PT samples clamped, i.e., constant strain conditions, would not degrade the performance when T_{hot} is set larger than T_{Curie} and (ii) piezoelectric properties such as d_{33} are important in materials transitioning from one ferroelectric phase to another.

Finally, the tetragonal to cubic phase transition is the most interesting because unlike the ferroelectric phase transitions, ferroelectric-to-paraelectric transition results in complete depolarization of the material [23]. For PMN–32PT, the largest polarization change was observed between 80 and 170 °C which resulted in the largest amount of energy harvested. Furthermore, the energy density harvested N_D featured a non-linear relation with temperature T_{hot} as illustrated in figure 3. In fact, the energy density increased by approximately 24 mJ cm^{-3}/cycle when T_{hot} increased from 140 to 150 °C compared with 9 mJ cm^{-3}/cycle when T_{hot} increased from 160 to 170 °C. This indicates a large gain in energy density when T_{hot} was set around T_{Curie} confirming the importance of the ferro-to-paraelectric transition on pyroelectric energy conversion. Furthermore, the increase in energy density was minimal when T_{hot} was increased from 160 to 170 °C due to complete depolarization of the material above T_{Curie}. Increasing T_{hot} beyond 170 °C would not result in any significant increase on the amount of energy harvested and therefore was not considered in this study.

5.1.2. Effect of electric fields E_L and E_H. This section discusses the effects of the low and high electric fields E_L and E_H on the energy density N_D generated during the Olsen cycle. Increasing E_H led to an increase in the amount of energy harvested as previously stated and as illustrated in figure 3. This parameter was limited to 9 kV cm^{-1} corresponding to approximately the dielectric strength of the material.

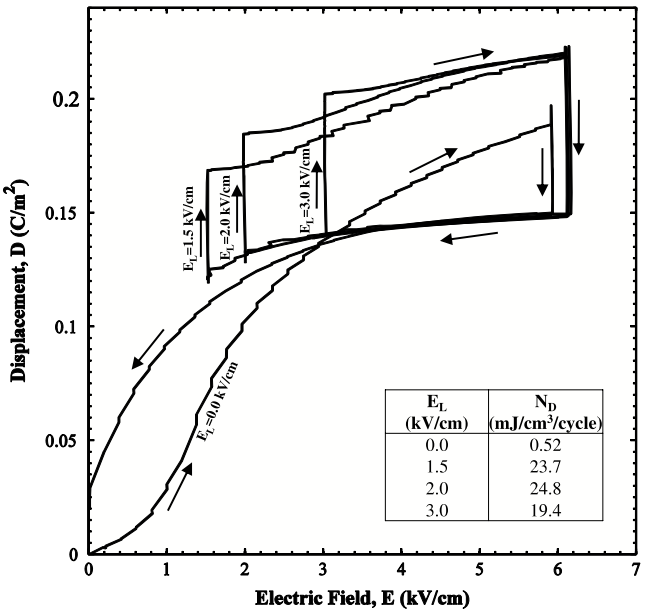

Figure 5. Experimental Olsen cycle diagrams performed on [001] poled PMN–32PT between $T_{cold} = 80\,^{\circ}C$ and $T_{hot} = 140\,^{\circ}C$ for $E_H = 6$ kV cm^{-1} and E_L varying from 0 to 3.0 kV cm^{-1}.

In order to investigate the effects of the low electric field E_L on the energy density, the Olsen cycle was performed between the temperatures $T_{cold} = 80\,^{\circ}C$ and $T_{hot} = 140\,^{\circ}C$ for $E_H = 6$ kV cm^{-1}. Figure 5 shows four different Olsen cycles in the *D*–*E* diagram performed with $E_L = 0$, 1.5, 2.0, and 3.0 kV cm^{-1}. The cycles are shown superimposed to facilitate their comparison. For the three cases when E_L was equal to 1.5, 2.0, and 3.0 kV cm^{-1}, the material reached approximately the same electric displacement when the electric field was raised to E_H at T_{cold}. By contrast, when E_L was set to 0 kV cm^{-1} the sample was unable to repolarize as the temperature decreased from T_{hot} to T_{cold} during process 4–1 (figure 1).

Moreover, the energy density harvested for different values of E_L are also summarized in the inset of figure 5. The optimal value of E_L was found to be 2.0 kV cm^{-1} with an energy density of 24.8 mJ cm^{-3}/cycle. Increasing E_L to 3.0 kV cm^{-1} resulted in smaller energy density due to the reduction in electric field span ($E_H - E_L$) despite the fact that the sample had larger polarization at E_L and T_{cold} (point 1 on figure 1). The energy density harvested when $E_L = 0$ kV cm^{-1} was 0.5 mJ cm^{-3}. This is significantly lower than that obtained when $E_L = 2$ kV cm^{-1} despite the fact that the electric field span ($E_H - E_L$) was larger. This can be attributed to the depoling of the sample at T_{cold} and E_L resulting in crossover of the two *D*–*E* curves.

5.2. Model predictions

Figure 3 compares the energy density obtained experimentally with that predicted (i) by equation (2) assuming constant properties with $p = 800$ μC m^{-2} K^{-1}, its value at 80 °C [34] and (ii) by equation (10) accounting for temperature dependent properties summarized in table 1. It indicates that the predictions of the constant-property model deteriorated as the

temperature difference $\Delta T = T_{hot} - T_{cold}$ increased. Indeed, the pyroelectric coefficient of PMN–32PT increases by an order of magnitude between 80 and 150 °C [34]. Thus, the constant properties model (equation (2)) understandably underpredicted the energy density harvested during the Olsen cycle. It also lacked a limit on the value of T_{hot}. Indeed, the pyroelectric coefficient of PMN–32PT was negligible beyond 170 °C which the model did not account for [34]. Note that the model has been used in the past to extrapolate results for T_{hot} larger than T_{Curie} by up to 60 °C [16]. However, as stated previously increasing T_{hot} from 160 to 170 °C resulted in minimal increase in energy density. As a result, linearly extrapolating the energy density to temperatures significantly above the Curie temperature results in exceedingly inaccurate predictions.

Furthermore, the effects of thermal expansion were taken into account by the temperature-dependent-property model (equation (10)) for T_{hot} =130 and 140 °C. However, they were neglected for $T_{hot} \geqslant 150$ °C as the terms x_3 and d_{33} are negligible as previously discussed. Figure 3 shows that reasonable agreement was found between this model's predictions and experimental data. In fact, the relative error was less than 20% for all values of temperatures and electric fields explored. This is remarkable given the fact that the properties used were obtained from the literature (table 1) and that material properties from one sample to the next showed variations estimated around ±20% in spontaneous polarization, relative permittivity, and Curie temperature [31]. In addition, the model presented here does not require knowledge of the pyroelectric coefficient in order to calculate the energy density generated by a ferroelectric material subjected to the Olsen cycle. However, this model does not simulate the hysteresis behavior and is valid in the region where the displacement depends linearly on the electric field. This is generally the case for the Olsen cycle and indeed was the case for the experiments performed on PMN–32PT with E_L larger than 2.0 kV cm^{-1}.

6. Conclusion

This study presented experimental measurements of energy density generated by commercial PMN–32PT capacitors subjected to the Olsen cycle. Physical models were also derived to predict the energy density of the cycle. The maximum energy density harvested with PMN–32PT was found to be 100 mJ cm^{-3}/cycle between temperatures T_{cold} = 80 °C and T_{hot} = 170 °C and electric field spanning from 2.0 to 9.0 kV cm^{-1}. The energy harvested due to rhombohedral to tetragonal phase transition alone was found to be 55 mJ cm^{-3}/cycle operating between the temperatures T_{cold} = 80 °C and T_{hot} = 140 °C. Moreover, the optimal value of E_L resulting in the highest energy density was 2 kV cm^{-1}. Finally, a simple temperature dependent properties model (equation (10)) was able to predict experimental measurements within 20% for a wide range of temperatures and electric fields. The performance of the PMN–32PT was similar to previously used ceramic and single crystal relaxor ferroelectrics [16–19]. However, unlike most previous studies, the PMN–32PT samples used in the present study were commercially available.

Acknowledgment

This research has been supported in part by the NSF-IGERT program 'Clean Energy for Green Industry at UCLA' (DGE-0903720).

References

[1] Lawrence Livermore National Laboratory 2010 *US Energy Flow Trends—2009* https://publicaffairs.llnl.gov/news/energy/energy.html#2009 accessed September 21
[2] Shioji M, Ishiyama T, Ikegami M, Mitani S and Shibata H 2001 Performance and exhaust emissions in a natural-gas fueled dual-fuel engine *JSME Int. J.* B **44** 641–8
[3] Avallone E 1987 *Marks' Standard Handbook for Mechanical Engineers* 9th edn (New York: McGraw-Hill)
[4] Riffat S B and Ma X 2003 Thermoelectrics: a review of present and potential applications *Appl. Therm. Eng.* **23** 913–35
[5] Olsen R B and Bruno D A 1986 Pyroelectric conversion materials *Proc. 21st Intersociety Energy Conversion Engineering Conf. (Aug. 1986)* (San Diego, CA: American Chemical Society) pp 89–93
[6] Olsen R B, Bruno D A and Briscoe J M 1984 Cascaded pyroelectric energy converter *Ferroelectrics* **59** 205–19
[7] Olsen R B, Bruno D A and Briscoe J M 1985 Pyroelectric conversion cycles *J. Appl. Phys.* **58** 4709–16
[8] Olsen R B, Bruno D A, Briscoe J M and Butler W F 1981 A pyroelectric energy converter which employs regeneration *Ferroelectrics* **38** 975–8
[9] Olsen R B 1982 Ferroelectric conversion of heat to electrical energy—a demonstration *J. Energy* **6** 91–5
[10] Olsen R B and Brown D D 1982 High-efficiency direct conversion of heat to electrical energy, related pyroelectric measurements *Ferroelectrics* **40** 17–27
[11] Kouchachvili L and Ikura M 2008 Improving the efficiency of pyroelectric conversion *Int. J. Energy Res.* **32** 328–35
[12] Kouchachvili L and Ikura M 2006 High performance P(VDF-TrFE) copolymer for pyroelectric conversion *US Patent Specification* 7,323,506
[13] Ikura M 2002 Conversion of low-grade heat to electricity using pyroelectric copolymer *Ferroelectrics* **267** 403–8
[14] Navid A, Vanderpool D, Bah A and Pilon L 2010 Towards optimization of a pyroelectric energy converter for harvesting waste heat *Int. J. Heat Mass Transfer* **53** 4060–70
[15] Navid A and Pilon L 2010 Pyroelectric energy harvesting using olsen cycles in purified and porous poly(vinylidene fluoride-trifuoroethylene) thin films *Smart Mater. Struct.* **20** 025012
[16] Sebald G, Seveyrat L, Guyomar D, Lebrun L, Guiffard B and Pruvost S 2006 Electrocaloric and pyroelectric properties of 0.75Pb($Mg_{1/3}Nb_{2/3}$)O_3–0.25$PbTiO_3$ single crystals *J. Appl. Phys.* **100** 124112
[17] Guyomar D, Pruvost S and Sebald G 2008 Energy harvesting based on FE–FE transition in ferroelectric single crystals *IEEE Trans. Ultrason. Ferroelectr. Freq. Control* **55** 279–85
[18] Khodayari A, Pruvost S, Sebald G, Guyomar D and Mohammadi S 2009 Nonlinear pyroelectric energy harvesting from relaxor single crystals *IEEE Trans. Ultrason. Ferroelectr. Freq. Control* **56** 693–9
[19] Zhu H, Pruvost S, Guyomar D and Khodayari A 2009 Thermal energy harvesting from $Pb(Zn_{1/3}Nb_{2/3})_{0.955}Ti_{0.045}O_3$ single crystals phase transitions *J. Appl. Phys.* **106** 124102
[20] Fang J, Frederich H and Pilon L 2010 Harvesting nanoscale thermal radiation using pyroelectric materials *ASME J. Heat Transfer* **132** 092701
[21] Nguyen H, Navid A and Pilon L 2010 Improved pyroelectric energy converter for waste heat energy harvesting using co-polymer P(VDF-TrFE) and Olsen cycle *Appl. Thermal Eng.* **30** 2127–37

[22] Cuadras A, Gasulla M and Ferrari V 2010 Thermal energy harvesting through pyroelectricity *Sensors Actuators* A **158** 132–9
[23] Lang S B and Das-Gupta D K 2001 *Handbook of Advanced Electronic and Photonic Materials and Devices* vol 4 (San Diego, CA: Academic)
[24] Lines M E and A M Glass 1977 *Principles and Applications of Ferroelectrics and Related Materials* (Oxford: Clarendon)
[25] Samara G A 2001 Ferroelectricity revisited-advances in materials and physics *Solid State Physics* vol 56 (San Diego, CA: Academic) pp 239–458
[26] Li Z, Xi Z, Xu Z and Yao X 2002 Dielectric/ferroelectric response and phase transition of PMN0.32PT single crystal *J. Mater. Sci. Lett.* **21** 1325–7
[27] Moran M J and Shapiro H N 2004 *Fundamentals of Engineering Thermodynamics* 5th edn (New York: Wiley)
[28] Olsen R B, Bruno D A and Briscoe J M 1985 Pyroelectric conversion cycle of vinylidene fluoride-trifluoroethylene copolymer *J. Appl. Phys.* **57** 5036–42
[29] Vanderpool D, Yoon J H and Pilon L 2008 Simulations of a prototypical device using pyroelectric materials for harvesting waste heat *Int. J. Heat Mass Transfer* **51** 5052–62
[30] Sebald G, Pruvost S and Guyomar D 2008 Energy harvesting based on Ericsson pyroelectric cycles in a relaxor ferroelectric ceramic *Smart Mater. Struct.* **17** 015012
[31] Sinoceramics L L C 2011 *Sinoceramics PMN–PT Single Crystal* http://www.sinocera.com/single%20crystal-pmn%20pt%20crystal.htm accessed February 19
[32] Li Z, Xu Z, Xi Z, Xiang F and Yao X 2007 Thermal expansion characteristics in [001]-oriented PMN–0.32PT single crystals *Ferroelectrics* **355** 245–51
[33] Yasuda N, Banno T, Fujita K, Ohwa H, Matushita M, Yamashita Y, Iwata M and Ishibashi Y 2007 Piezoelectric properties of relaxor ferroelectric solid solution single crystals PMN–PT and PZN–PT near MPB under pressures *Ferroelectrics* **347** 44–9
[34] Kumar P, Sharma S, Thakur O P, Prakash C and Goel T C 2004 Dielectric, piezoelectric and pyroelectric properties of PMN–PT (68:32) system *Ceram. Int.* **30** 585–9
[35] Mischenko A S, Zhang Q, Whatmore R W, Scott J F and Mathur N D 2006 Giant electrocaloric effect in the thin film relaxor ferroelectric 0.9 $PbMg_{1/3}Nb_{2/3}O_3$–0.1 $PbTiO_3$ near room temperature *Appl. Phys. Lett.* **89** 242912